



PERGAMON

Journal of Quantitative Spectroscopy &  
Radiative Transfer 72 (2002) 201–225

---

---

Journal of  
Quantitative  
Spectroscopy &  
Radiative  
Transfer

---

---

www.elsevier.com/locate/jqsrt

# Properties of reflected sunlight derived from a Green's function method

A. Benedetti\*, P. Gabriel, G.L. Stephens

*Department of Atmospheric Science, Colorado State University, Fort Collins, CO 80523, USA*

Received 11 August 2000

---

## Abstract

The inference of optical depth and particle size of clouds and aerosols using remotely sensed reflected radiance at solar wavelengths has received much attention recently. The information these measurements provide is path integrated. However, very little is known about the vertical distribution of this weighting. To characterize it, we first solve the radiative transfer equation (RTE) by a Green's function approach, and then investigate the sensitivity of the weighting to vertical inhomogeneities in the extinction by introducing a function that is closely related to the Green's function, herein called the contribution function. This function calculates the contributions to the radiance at the upper boundary of the medium by underlying layers. Three hypothetical clouds of identical optical depth but exhibiting different extinction profiles were used in this study. The contribution function was found very sensitive to the extinction profile. The global reflection and transmission matrices used to construct the Green's function, derived using an eigenmatrix method, resulted in an efficient, stable, and accurate method for calculating the emerging radiances that can be extended to multi-layered media. © 2001 Elsevier Science Ltd. All rights reserved.

---

## 1. Introduction

Measurements of sunlight scattered in the Earth's atmosphere are used to infer information about cloud and aerosol particles as well as information about the abundance of trace gases in the atmosphere. Retrieval methods developed to infer optical depth and particle size of clouds and aerosol using observations of solar reflectance typically rely on measurements in two or sometimes more spectral regions or bands (e.g. [1,2]). This approach yields path integrated information that is weighted in some way according to the distribution of particles along the

---

\* Corresponding author. Tel.: +1-970-491-3430; fax: +1-970-491-8166.

*E-mail address:* angela@reef.atmos.colostate.edu (A. Benedetti).

path. The weighting accounts for the vertical transport through plane parallel layers in a manner that quantifies the relative information content of each layer to the overall reflected or transmitted signal. A description of the nature of this path weighting of information has been given by Platnick [2].

The present work extends and generalizes his characterization of the weighting by using a Green's function formulation to calculate contributions to the radiance emerging at the upper boundary of a vertically inhomogeneous medium with a constant single scattering albedo. This solution provides, in a straightforward manner, a way of investigating the sensitivity of these contributions to the prescribed inhomogeneities (such as the vertical variations of the extinction or scattering functions) as a continuous function of the vertical coordinate.

Although many different techniques have been developed to solve the radiative transfer equation (e.g. [3]), the doubling–adding method (DA) (e.g. [4,5]) and the eigenmatrix formulation (e.g. discrete ordinate radiative transfer, DISORT [6]) are the most commonly used methods for dealing with vertically inhomogeneous media.

The eigenmatrix method solves the RTE by first discretizing the angular variation in the phase function and radiance, and then treating the resulting system of equations as a two-point boundary value problem (BVP). For vertically uniform optical properties, eigenmatrix methods are used to construct its solution. This method dates back to Chandrasekar [7]. The DA method solves the RTE by converting the two-point BVP into an initial value problem (IVP) via a Riccati transformation; this introduces the concept of global reflection ( $\mathcal{R}$ ) and global transmission ( $\mathcal{T}$ ) operators, that account for multiple reflections in a layer. For a single layer, homogenous in its optical properties, the DA method is reduced to simple doubling. For multi-layered media, the interaction principle is used to compute the global reflection and transmission matrices for the whole medium via the adding technique, once  $\mathcal{R}$  and  $\mathcal{T}$  for all layers are known.

The connection between the eigenmatrix and the DA method of solution was described by Waterman [8]. In that work he used the interaction principle to relate the matrix exponential to the global reflection and transmission operators. However, the computation of global  $\mathcal{R}$  and  $\mathcal{T}$  were approximated for thin ( $\tau < 1$ ) media, due to numerical instabilities encountered in thicker media. In this paper we reformulate Waterman's work by calculating  $\mathcal{R}$  and  $\mathcal{T}$  without approximation via the eigenmatrix approach in a manner that yields a numerically stable solution for any arbitrary optical depth. Subsequently, these stable forms for  $\mathcal{R}$  and  $\mathcal{T}$  are used to compute the Green's function, from which the goals stated above can be attained. This approach has received some attention in astrophysics (e.g. [9]) and in hydrologic optics (e.g. [10]).

The outline of the paper is as follows. Section 2 introduces a stable semi-analytical form for global  $\mathcal{R}$  and  $\mathcal{T}$  derived from the matrix exponential solution of the sourceless RTE. The solar source function is then added and the Green's function is derived in terms of the global  $\mathcal{R}$  and  $\mathcal{T}$ . Section 3 explores the numerical solution of the azimuthally dependent radiances for a single layer medium using the methods described in Section 2. Results are compared against a standard doubling code. The *Contribution Function* and its integral, the *Integrated Contribution Function*, are also introduced using the Green's function solution. We show vertical profiles of these functions and discuss their implications toward inferring extinction profiles from reflected solar radiation. This issue is further addressed by exploring the extent to which different portions

of the medium contribute to the observed radiances at the boundary. This is quantified in Section 4 via the simple concept of *penetration optical depth*. A summary and conclusion are provided in Section 5 along with a discussion of the physical significance of these results to the inverse problem of radiative transfer.

## 2. Theoretical foundations

### 2.1. Basic concepts

This study is posed in terms of the radiative transfer through a single isolated layer of an absorbing and scattering medium that possesses a prescribed vertical variation of optical properties. The layer will be taken to extend vertically from  $z = 0$  to  $H$ . The extension to a multi-layered medium is possible by a repeated application of the interaction principle for each layer, provided that the single scattering albedo  $\omega_0$  is constant in every layer. The solution for the  $i$ th layer is propagated as a boundary condition for the  $(i + 1)$ th layer in exactly the same manner as in the DA method. The resulting form of the solution will be invariant with respect to the number of layers.

#### 2.1.1. Discretization of the radiative transfer equation

Under the assumption that the single layer optical medium is horizontally homogeneous, the transfer of monochromatic diffuse radiation through the layer is governed by the plane-parallel equation of radiative transfer:

$$\mu \frac{dI(z, \mu, \phi)}{dz} = -\sigma_e(z)I(z, \mu, \phi) + \frac{\sigma_s(z)}{4\pi} \int_0^{2\pi} \int_{-1}^1 P(z, \mu, \phi, \mu', \phi') I(z, \mu', \phi') d\mu' d\phi' + \Sigma(z, \mu, \phi), \quad (1)$$

where  $I(z, \mu, \phi)$  is the specific intensity at level  $z$  along the direction specified by  $\mu$  (cosine of the polar angle) and  $\phi$  (azimuth angle),  $\sigma_e$  is the extinction function,  $\sigma_s$  the scattering function,  $P(z, \mu, \phi, \mu', \phi')$  is the phase function, and  $\Sigma(z, \mu, \phi)$  is the source.

To approximate the solution to (1) we discretize the integro-differential equation and then solve the resulting boundary value problem (BVP) with the boundary condition given in Section 3.1 by combining eigenmatrix and interaction principle methods. With the radiance written as

$$I(z, \mu, \phi) = \sum_{m=0}^M I_m(z, \mu) \cos [m(\phi - \phi_\odot)], \quad (2)$$

where  $\phi_\odot$  is the solar azimuth angle, and with similar expansions for the source term and the phase function in conjunction with Eq. (2), we obtain a system of  $M$  *uncoupled* equations, one for each term of the azimuthal expansion. Thus, the solution of (1) reduces to the solution of  $m$  BVPs. The radiance field can be divided into  $N$  upwelling and  $N$  downwelling *streams* for

each mode  $m$ , producing radiance vector pairs  $I_m^+(z)$  and  $I_m^-(z)$ . The RTE equation thus reduces to its fully discrete matrix form:

$$\frac{d}{dz} \begin{pmatrix} I_m^+(z) \\ I_m^-(z) \end{pmatrix} = \begin{pmatrix} \hat{\mathbf{t}}_m(z) & -\hat{\mathbf{r}}_m(z) \\ \hat{\mathbf{r}}_m(z) & -\hat{\mathbf{t}}_m(z) \end{pmatrix} \begin{pmatrix} I_m^+(z) \\ I_m^-(z) \end{pmatrix} + \begin{pmatrix} \hat{\Sigma}_m^+(z) \\ \hat{\Sigma}_m^-(z) \end{pmatrix}, \tag{3}$$

where  $\hat{\mathbf{t}}_m(z)$  and  $\hat{\mathbf{r}}_m(z)$  represent the local transmission and reflection matrices

$$\hat{\mathbf{t}}_m(z) = -\sigma_e(z)\mathbf{M} + \frac{(\mathbf{I} + \delta_{0,m})}{4}\sigma_s(z)\mathbf{M}\mathbf{P}_m^+\mathbf{W}, \tag{4}$$

$$\hat{\mathbf{r}}_m(z) = -\frac{(\mathbf{I} + \delta_{0,m})}{4}\sigma_s(z)\mathbf{M}\mathbf{P}_m^-\mathbf{W}. \tag{5}$$

$\mathbf{M}$  is the diagonal matrix whose elements are the inverse of cosines of the quadrature angles,  $\mathbf{W}$  is the diagonal matrix whose elements are the quadrature weights and  $\mathbf{P}_m^+$  and  $\mathbf{P}_m^-$  are the forward (+) and backward (–) phase function matrices, specified for a given  $m$ .  $\mathbf{I}$  is the unit matrix.

The source of diffuse radiation at solar wavelength can be written as

$$\hat{\Sigma}_m^\pm(z) = \frac{\sigma_s(z)}{4\pi}F_\odot\mathbf{M}\mathbf{P}_{\odot m}^\mp e^{-\int_z^H \sigma_e(z') dz'/\mu_\odot}, \tag{6}$$

where  $\mathbf{P}_{\odot m}^\mp$  are the forward and backward phase function vectors associated with scattering of the direct solar beam.  $F_\odot$  represents the monochromatic irradiance incident at the top of the layer and the exponential factor is the attenuation of this direct beam to the level  $z$  of interest.

### 2.1.2. Solution of the RTE for a vertically inhomogeneous layer

The usual method of solving (3) for a vertically varying optical medium is to divide the atmosphere into a number of distinct but vertically uniform layers. We develop an alternative solution to (3) for given specific analytical forms of the vertical variation of the extinction. The solution proceeds under the assumption that the single scattering albedo is constant through the layer. This is reasonable for wavelengths in the visible and near-infrared region of the spectrum.

The profile of the extinction function is defined as  $\sigma_e(z) = d\psi(z)/dz$  and by  $\sigma_s(z) = \omega_0(d\psi(z)/dz)$  where  $\omega_0$  is the single scattering albedo. The condition  $\sigma_e(z) > 0, \forall z$  must hold. This specific form of the extinction was chosen to simplify the integration of the exponential solution described below. We now redefine the source term and the local transmission and reflection matrices as

$$\hat{\Sigma}_m(z) = \frac{d\psi(z)}{dz}\Sigma_m(z), \tag{7}$$

$$\hat{\mathbf{t}}_m(z) = \frac{d\psi(z)}{dz}\mathbf{t}_m, \tag{8}$$

$$\hat{\mathbf{r}}_m(z) = \frac{d\psi(z)}{dz}\mathbf{r}_m, \tag{9}$$

where  $\mathbf{t}_m$  and  $\mathbf{r}_m$  are the local reflection and transmission matrices defined for constant coefficients, and  $\Sigma_m^\pm(z)$  is given by

$$\Sigma_m^\pm(z) = \frac{\omega_0}{4\pi} F_\odot \mathbf{M} \mathbf{P}_\odot^\mp e^{-\int_z^H \sigma_c(z') dz' / \mu_\odot}. \tag{10}$$

Using Eqs. (7)–(10) we now rewrite Eq. (3):

$$\frac{d}{dz} \begin{pmatrix} l_m^+(z) \\ l_m^-(z) \end{pmatrix} = \frac{d\psi(z)}{dz} \mathbf{A} \begin{pmatrix} l_m^+(z) \\ l_m^-(z) \end{pmatrix} + \frac{d\psi(z)}{dz} \begin{pmatrix} \Sigma_m^+(z) \\ \Sigma_m^-(z) \end{pmatrix}, \tag{11}$$

where we have introduced the  $(2N \times 2N)$  matrix:

$$\mathbf{A}_m = \begin{pmatrix} \mathbf{t}_m & -\mathbf{r}_m \\ \mathbf{r}_m & -\mathbf{t}_m \end{pmatrix}. \tag{12}$$

The integral solution to (11) thus follows as

$$\begin{pmatrix} l_m^+(H) \\ l_m^-(H) \end{pmatrix} = e^{\mathbf{A}_m \psi(H)} \begin{pmatrix} l_m^+(0) \\ l_m^-(0) \end{pmatrix} + \int_0^H e^{\mathbf{A}_m [\psi(H) - \psi(z)]} \begin{pmatrix} \Sigma_m^+ \\ \Sigma_m^- \end{pmatrix} \frac{d\psi(z)}{dz} dz, \tag{13}$$

where  $l_m^\pm(0)$  are the boundary conditions, and  $\psi(z)$  represents the integral with respect to  $z$  of the extinction coefficient.  $\psi(H)$  is the total optical depth, which in remote sensing literature is also indicated with the symbol  $\tau$ . In the following discussion, the two symbols are interchangeable.

To simplify the notation, hereafter the subscript  $m$  is dropped and all dependence on azimuth mode is understood.

### 2.1.3. Properties of the exponential matrix

A key step in evaluating (13) is the evaluation of the exponential matrix  $e^{\mathbf{A}\psi(z)}$ , and for this purpose it is convenient to *diagonalize*  $\mathbf{A}$ . From linear algebra we know that a square matrix  $\mathbf{A}$  gives rise to the eigenvalue problem

$$\mathbf{A}\mathbf{X} = \mathbf{X}\mathbf{\Lambda}, \tag{14}$$

where  $\mathbf{X}$  is the matrix whose columns are the *eigenvectors* of  $\mathbf{A}$  and  $\mathbf{\Lambda}$  is the diagonal matrix whose elements are the *eigenvalues* of  $\mathbf{A}$ . It is well known that the eigenvalues of the  $\mathbf{A}$  matrix are real and come in pairs  $(\pm\lambda_k, k = 1, \dots, N)$  (e.g. [11]).

From Eq. (14), it follows that

$$\mathbf{A} = \mathbf{X}\mathbf{\Lambda}\mathbf{X}^{-1}. \tag{15}$$

By expanding the matrix exponential in a Taylor series of the variable  $\psi(z)$ , we have

$$e^{\mathbf{A}\psi(z)} = \mathbf{X} e^{\mathbf{\Lambda}\psi(z)} \mathbf{X}^{-1}, \tag{16}$$

where  $e^{\mathbf{\Lambda}\psi(z)}$  is a diagonal matrix. The solution of the RTE is thus reduced to computing the eigenvalues and eigenvectors of  $\mathbf{A}$ . As is known, this task poses numerical difficulties, but the form of  $\mathbf{A}$  can be exploited to reduce the order of the problem from  $2N$  to  $N$  by applying the technique of *deflation of polynomial degree* [12]. This not only reduces the computational

time, but offers insight into the underlying structure of the exponential matrix itself. Details of this approach applied to the matrix  $\mathbf{A}$  are presented in Appendix A.

Using the spectral decomposition of  $\mathbf{A}$  and the two matrices

$$\mathbf{X} = \begin{pmatrix} \mathbf{u}_+ & \mathbf{u}_- \\ -\mathbf{u}_- & -\mathbf{u}_+ \end{pmatrix}$$

and

$$\mathbf{X}^{-1} = \begin{pmatrix} \mathbf{v}_+ & \mathbf{v}_- \\ -\mathbf{v}_- & -\mathbf{v}_+ \end{pmatrix},$$

where from Appendix A we have

$$\begin{aligned} \mathbf{v}_+ &= [\mathbf{I} - (\mathbf{u}_+^{-1}\mathbf{u}_-)^2]^{-1}\mathbf{u}_+^{-1}, \\ \mathbf{v}_- &= (\mathbf{u}_+^{-1}\mathbf{u}_-)\mathbf{v}_+, \end{aligned}$$

we can write the exponential matrix as follows:

$$\begin{aligned} \mathbf{X}e^{\Lambda\psi(z)}\mathbf{X}^{-1} &= \begin{pmatrix} \mathbf{u}_+ & \mathbf{u}_- \\ -\mathbf{u}_- & -\mathbf{u}_+ \end{pmatrix} \begin{pmatrix} e^{\Lambda^+\psi(z)} & \mathbf{0} \\ \mathbf{0} & e^{-\Lambda^+\psi(z)} \end{pmatrix} \begin{pmatrix} \mathbf{v}_+ & \mathbf{v}_- \\ -\mathbf{v}_- & -\mathbf{v}_+ \end{pmatrix} \\ &= \begin{pmatrix} \mathbf{e}_{11}(z) & \mathbf{e}_{12}(z) \\ \mathbf{e}_{21}(z) & \mathbf{e}_{22}(z) \end{pmatrix}, \end{aligned} \tag{17}$$

where

$$\mathbf{e}_{11}(z) = \mathbf{u}_+e^{\Lambda^+\psi(z)}\mathbf{v}_+ - \mathbf{u}_-e^{-\Lambda^+\psi(z)}\mathbf{v}_-, \tag{18}$$

$$\mathbf{e}_{12}(z) = \mathbf{u}_+e^{\Lambda^+\psi(z)}\mathbf{v}_- - \mathbf{u}_-e^{-\Lambda^+\psi(z)}\mathbf{v}_+, \tag{19}$$

$$\mathbf{e}_{21}(z) = -\mathbf{u}_-e^{\Lambda^+\psi(z)}\mathbf{v}_+ + \mathbf{u}_+e^{-\Lambda^+\psi(z)}\mathbf{v}_-, \tag{20}$$

$$\mathbf{e}_{22}(z) = -\mathbf{u}_-e^{\Lambda^+\psi(z)}\mathbf{v}_- + \mathbf{u}_+e^{-\Lambda^+\psi(z)}\mathbf{v}_+. \tag{21}$$

Here  $\Lambda^+$  is the diagonal matrix corresponding to the *positive* eigenvalues of  $\mathbf{A}$ .

Thus, the elements of the eigenmatrix are linear combinations of decaying and growing exponentials. The growing exponentials are a source of numerical instability when  $\psi(z)$  becomes large. This instability can be circumvented by using the interaction form of the solution to (11) which requires the specification of the global reflection and transmission matrices.

### 2.2. Global reflection and transmission matrices

Recasting the eigenmatrix solution into the form of the interaction principle leads to a direct derivation of the global transmission and reflection operators. Using the interaction principle for a single layer of depth  $H$ , and in the absence of sources, we can write:

$$\begin{aligned} \mathbf{l}^+(H) &= \mathcal{T}(0,H)\mathbf{l}^+(0) + \mathcal{R}(H,0)\mathbf{l}^-(H), \\ \mathbf{l}^-(0) &= \mathcal{R}(0,H)\mathbf{l}^+(0) + \mathcal{T}(H,0)\mathbf{l}^-(H), \end{aligned} \tag{22}$$

where  $\mathcal{T}(0, H)$  and  $\mathcal{R}(0, H)$  are the global transmission and reflection functions for illumination from below, and  $\mathcal{T}(H, 0)$  and  $\mathcal{R}(H, 0)$  are for illumination from above.

From the homogeneous solution of the RTE (first term on right-hand side of Eq. (13)) we have

$$\begin{aligned} \begin{pmatrix} I^+(H) \\ I^-(H) \end{pmatrix} &= \mathbf{X}e^{\Lambda\psi(H)}\mathbf{X}^{-1} \begin{pmatrix} I^+(0) \\ I^-(0) \end{pmatrix} \\ &= \begin{pmatrix} \mathbf{e}_{11}(H) & \mathbf{e}_{12}(H) \\ \mathbf{e}_{21}(H) & \mathbf{e}_{22}(H) \end{pmatrix} \begin{pmatrix} I^+(0) \\ I^-(0) \end{pmatrix}, \end{aligned} \tag{23}$$

which can be rewritten as

$$\begin{aligned} I^+(H) &= \mathbf{e}_{11}(H)I^+(0) + \mathbf{e}_{12}(H)I^-(0), \\ I^-(H) &= \mathbf{e}_{21}(H)I^+(0) + \mathbf{e}_{22}(H)I^-(0). \end{aligned} \tag{24}$$

Solving for  $I^-(0)$  and  $I^+(H)$ , gives

$$\begin{aligned} I^+(H) &= [\mathbf{e}_{11}(H) - \mathbf{e}_{12}(H)\mathbf{e}_{22}^{-1}(H)\mathbf{e}_{21}(H)]I^+(0) + \mathbf{e}_{12}(H)\mathbf{e}_{22}^{-1}(H)I^-(0), \\ I^-(0) &= \mathbf{e}_{22}^{-1}(H)I^-(H) - \mathbf{e}_{22}^{-1}(H)\mathbf{e}_{21}(H)I^+(0). \end{aligned} \tag{25}$$

Comparing Eq. (22) to Eq. (25) we establish that:

$$\mathcal{T}(0, H) = \mathbf{e}_{11}(H) - \mathbf{e}_{12}(H)\mathbf{e}_{22}^{-1}(H)\mathbf{e}_{21}(H), \tag{26}$$

$$\mathcal{R}(H, 0) = \mathbf{e}_{12}(H)\mathbf{e}_{22}^{-1}(H), \tag{27}$$

$$\mathcal{T}(H, 0) = \mathbf{e}_{22}^{-1}(H), \tag{28}$$

$$\mathcal{R}(0, H) = -\mathbf{e}_{22}^{-1}(H)\mathbf{e}_{21}(H). \tag{29}$$

Thus, the global reflection and transmission matrices are completely determined from linear combinations of elements of the eigenmatrix. In principle, these matrices are stable over all ranges of optical depth. However, the form of Eqs. (26)–(29) remains unstable. The steps toward achieving a stable form of  $\mathcal{R}$  and  $\mathcal{T}$  are discussed in Appendix B. With the development described there, the stable forms of these matrices are

$$\mathcal{T}(H, 0) = -\mathbf{u}_+[\mathbf{I} - (\mathbf{u}_+^{-1}\mathbf{u}_-)^2][(\mathbf{u}_+^{-1}\mathbf{u}_-)^{-1}e^{-\Lambda^+\psi(H)}]\{\mathbf{I} - [(\mathbf{u}_+^{-1}\mathbf{u}_-)^{-1}e^{-\Lambda^+\psi(H)}]^2\}^{-1}\mathbf{u}_-^{-1} \tag{30}$$

and

$$\begin{aligned} \mathcal{R}(H, 0) &= -\mathbf{u}_+[\mathbf{I} - (\mathbf{u}_+^{-1}\mathbf{u}_-)^{-1}e^{-\Lambda^+\psi(H)}](\mathbf{u}_+^{-1}\mathbf{u}_-)^{-1}e^{-\Lambda^+\psi(H)} \\ &\quad \{\mathbf{I} - [(\mathbf{u}_+^{-1}\mathbf{u}_-)^{-1}e^{-\Lambda^+\psi(H)}]^2\}^{-1}\mathbf{u}_-^{-1}. \end{aligned} \tag{31}$$

For a layer of constant  $\omega_0$ , even though  $\sigma_e(z)$  and  $\sigma_s(z)$  are varying as assumed in this work,  $\mathcal{R}(H, 0) = \mathcal{R}(0, H)$  and  $\mathcal{T}(H, 0) = \mathcal{T}(0, H)$ .

A direct numerical comparison with the global reflection and transmission matrices derived using doubling showed that both  $\mathcal{R}$  and  $\mathcal{T}$ , calculated using single precision, are stable up to a total optical depth of 1000. This technique allows for the evaluation of global  $\mathcal{T}$  and  $\mathcal{R}$  for the entire layer without any approximation or first order expansion. When the source terms are taken into account, the radiance exiting the top of the layer can be computed efficiently and accurately.

### 2.3. Derivation of the Green's function matrix

In this section, we will use the interaction principle and the global reflection and transmission matrices developed above to compute the Green's function. The solution to the RTE equation with sources may be written as

$$\begin{aligned} \begin{pmatrix} I^+(H) \\ I^-(H) \end{pmatrix} &= \mathbf{X} e^{\Lambda \psi(H)} \mathbf{X}^{-1} \begin{pmatrix} I^+(0) \\ I^-(0) \end{pmatrix} + \begin{pmatrix} J^+ \\ J^- \end{pmatrix} \\ &= \begin{pmatrix} \mathbf{e}_{11}(H) & \mathbf{e}_{12}(H) \\ \mathbf{e}_{21}(H) & \mathbf{e}_{22}(H) \end{pmatrix} \begin{pmatrix} I^+(0) \\ I^-(0) \end{pmatrix} + \begin{pmatrix} J^+ \\ J^- \end{pmatrix}, \end{aligned} \tag{32}$$

where the source term is given by the following integral:

$$J^\pm = \int_0^H e^{\Lambda[\psi(H)-\psi(z)]} \begin{pmatrix} \Sigma^+ \\ \Sigma^- \end{pmatrix} \frac{d\psi(z)}{dz} dz. \tag{33}$$

If we rewrite the solution in the interaction principle form, and substitute the global  $\mathcal{R}$  and  $\mathcal{T}$  matrices, we have

$$\begin{pmatrix} I^+(H) \\ I^-(0) \end{pmatrix} = \begin{pmatrix} \mathcal{T}(0, H) & \mathcal{R}(H, 0) \\ \mathcal{R}(0, H) & \mathcal{T}(H, 0) \end{pmatrix} \begin{pmatrix} I^+(0) \\ I^-(H) \end{pmatrix} + \begin{pmatrix} \mathbf{I} & -\mathcal{R}(H, 0) \\ \mathbf{0} & -\mathcal{T}(H, 0) \end{pmatrix} \begin{pmatrix} J^+ \\ J^- \end{pmatrix}. \tag{34}$$

Since global  $\mathcal{R}$  and  $\mathcal{T}$  do not depend on  $z$ , we can bring the matrix inside the integral that defines the source term and proceed to multiply the two matrices:

$$\begin{aligned} &\begin{pmatrix} \mathbf{I} & -\mathcal{R}(H, 0) \\ \mathbf{0} & -\mathcal{T}(H, 0) \end{pmatrix} e^{\Lambda(\psi(H)-\psi(z))} \\ &= \begin{pmatrix} \mathbf{I} & -\mathcal{R}(H, 0) \\ \mathbf{0} & -\mathcal{T}(H, 0) \end{pmatrix} \begin{pmatrix} \mathbf{e}_{11}(H-z) & \mathbf{e}_{12}(H-z) \\ \mathbf{e}_{21}(H-z) & \mathbf{e}_{22}(H-z) \end{pmatrix} \\ &= \begin{pmatrix} \mathbf{e}_{11}(H-z) - \mathcal{R}(H, 0)\mathbf{e}_{21}(H-z) & \mathbf{e}_{12}(H-z) - \mathcal{R}(H, 0)\mathbf{e}_{22}(H-z) \\ -\mathcal{T}(H, 0)\mathbf{e}_{21}(H-z) & -\mathcal{T}(H, 0)\mathbf{e}_{22}(H-z) \end{pmatrix} \\ &= \begin{pmatrix} \mathbf{G}_{++}(H-z) & \mathbf{G}_{+-}(H-z) \\ \mathbf{G}_{-+}(H-z) & \mathbf{G}_{--}(H-z) \end{pmatrix} = \mathbf{G}(H-z). \end{aligned} \tag{35}$$

Expression (35) represents the Green’s function matrix for the RT problem. Since it contains  $\mathbf{e}_{11}$ ,  $\mathbf{e}_{12}$ ,  $\mathbf{e}_{21}$ , and  $\mathbf{e}_{22}$ , its form is numerically unstable for large optical depths. However, if we consider Eq. (35), the Green’s function matrix can be subdivided into four submatrices which contain decaying and growing exponentials. As before, we can manipulate each of these submatrices separately in an effort to induce stability.

Beginning with the top left corner submatrix  $\mathbf{G}_{++}(H-z)$ , if we write  $\mathbf{e}_{11}(H-z)$  and  $\mathbf{e}_{21}(H-z)$  explicitly we have

$$\begin{aligned} \mathbf{G}_{++}(H-z) &= \mathbf{e}_{11}(H-z) - \mathcal{R}(H,0)\mathbf{e}_{21}(H-z) \\ &= \mathbf{u}_+ \mathbf{e}^{\Lambda^+[\psi(H)-\psi(z)]} \mathbf{v}_+ - \mathbf{u}_- \mathbf{e}^{-\Lambda^+[\psi(H)-\psi(z)]} \mathbf{v}_- \\ &\quad - \mathcal{R}(H,0)(-\mathbf{u}_- \mathbf{e}^{\Lambda^+[\psi(H)-\psi(z)]} \mathbf{v}_+ + \mathbf{u}_+ \mathbf{e}^{-\Lambda^+[\psi(H)-\psi(z)]} \mathbf{v}_-) \\ &= \mathbf{u}_+ \mathbf{e}^{\Lambda^+[\psi(H)-\psi(z)]} \mathbf{v}_+ + \mathcal{R}(H,0)\mathbf{u}_- \mathbf{e}^{\Lambda^+[\psi(H)-\psi(z)]} \mathbf{v}_+ \\ &\quad - \mathbf{u}_- \mathbf{e}^{-\Lambda^+[\psi(H)-\psi(z)]} \mathbf{v}_- - \mathcal{R}(H,0)\mathbf{u}_+ \mathbf{e}^{-\Lambda^+[\psi(H)-\psi(z)]} \mathbf{v}_-. \end{aligned} \tag{36}$$

The reason for the regrouping of the matrices becomes evident by noting that the two terms which contains  $\mathbf{e}^{-\Lambda^+[\psi(H)-\psi(z)]}$  are inherently stable, since  $\Lambda^+$  is a diagonal matrix of all positive elements and by definition  $\psi(H) > \psi(z)$ ,  $\forall z < H$ . However, the two terms containing  $\mathbf{e}^{\Lambda^+[\psi(H)-\psi(z)]}$  are unstable.

We write these terms as

$$\begin{aligned} &\mathbf{u}_+ \mathbf{e}^{\Lambda^+[\psi(H)-\psi(z)]} \mathbf{v}_+ + \mathcal{R}(H,0)\mathbf{u}_- \mathbf{e}^{\Lambda^+[\psi(H)-\psi(z)]} \mathbf{v}_+ \\ &= \mathbf{u}_+ [\mathbf{I} + \mathbf{u}_+^{-1} \mathcal{R}(H,0)\mathbf{u}_-] \mathbf{e}^{-\Lambda^+[\psi(H)-\psi(z)]} \mathbf{v}_+. \end{aligned} \tag{37}$$

If we use global  $\mathcal{R}$  derived in Section 2.2 in the above expression, we can proceed to compute a stable form for (36):

$$\begin{aligned} \mathbf{G}_{++}(H-z) &= \mathbf{u}_+ \{ -[\mathbf{I} - ((\mathbf{u}_+^{-1}\mathbf{u}_-)^{-1} \mathbf{e}^{-\Lambda^+\psi(H)})^2]^{-1} (\mathbf{u}_+^{-1}\mathbf{u}_-)^{-1} \mathbf{e}^{-\Lambda^+\psi(H)} \\ &\quad + (\mathbf{u}_+^{-1}\mathbf{u}_-) \mathbf{e}^{-\Lambda^+\psi(H)} [\mathbf{I} - ((\mathbf{u}_+^{-1}\mathbf{u}_-)^{-1} \mathbf{e}^{-\Lambda^+\psi(H)})^2]^{-1} \} (\mathbf{u}_+^{-1}\mathbf{u}_-)^{-1} \mathbf{e}^{-\Lambda^+\psi(z)} \mathbf{v}_+ \\ &\quad - [\mathbf{u}_- + \mathcal{R}(H,0)\mathbf{u}_+] \mathbf{e}^{-\Lambda^+[\psi(H)-\psi(z)]} \mathbf{v}_-. \end{aligned} \tag{38}$$

This expression appears complex, but is numerically stable.

Similarly, we can divide the submatrix in the top right corner of (35)  $\mathbf{G}_{+-}(H - z)$ , into a stable part and an unstable part and stabilize the latter, making use again of the computed  $\mathcal{R}$ :

$$\begin{aligned} \mathbf{G}_{+-}(H - z) &= \mathbf{u}_+ \{ -[\mathbf{I} - ((\mathbf{u}_+^{-1}\mathbf{u}_-)^{-1}e^{-\Lambda^+\psi(H)})^2]^{-1}(\mathbf{u}_+^{-1}\mathbf{u}_-)^{-1}e^{-\Lambda^+\psi(H)} \\ &\quad + (\mathbf{u}_+^{-1}\mathbf{u}_-)e^{-\Lambda^+\psi(H)}[\mathbf{I} - ((\mathbf{u}_+^{-1}\mathbf{u}_-)^{-1}e^{-\Lambda^+\psi(H)})^2]^{-1} \} (\mathbf{u}_+^{-1}\mathbf{u}_-)^{-1}e^{-\Lambda^+\psi(z)}\mathbf{v}_- \\ &\quad - [\mathbf{u}_- + \mathcal{R}(H, 0)\mathbf{u}_+]e^{-\Lambda^+[\psi(H)-\psi(z)]}\mathbf{v}_+. \end{aligned} \tag{39}$$

For the submatrix in the bottom left of (35),  $\mathbf{G}_{-+}(H - z)$ , we can apply a similar procedure, this time using  $\mathcal{T}$  and obtain:

$$\begin{aligned} \mathbf{G}_{-+}(H - z) &= -\mathbf{u}_+[\mathbf{I} - (\mathbf{u}_+^{-1}\mathbf{u}_-)^2][\mathbf{I} - ((\mathbf{u}_+^{-1}\mathbf{u}_-)^{-1}e^{-\Lambda^+\psi(H)})^2]^{-1}(\mathbf{u}_+^{-1}\mathbf{u}_-)^{-1}e^{-\Lambda^+\psi(z)} \\ &\quad [\mathbf{I} - e^{-\Lambda^+[\psi(H)-\psi(z)]}(\mathbf{u}_+^{-1}\mathbf{u}_-)^{-1}e^{-\Lambda^+[\psi(H)-\psi(z)]}(\mathbf{u}_+^{-1}\mathbf{u}_-)]\mathbf{v}_+. \end{aligned} \tag{40}$$

For the submatrix in the bottom right corner of (35),

$$\begin{aligned} \mathbf{G}_{--}(H - z) &= -\mathbf{u}_+[\mathbf{I} - (\mathbf{u}_+^{-1}\mathbf{u}_-)^2][\mathbf{I} - ((\mathbf{u}_+^{-1}(\mathbf{u}_+^{-1}\mathbf{u}_-)^{-1}\mathbf{u}_-)^{-1}e^{-\Lambda^+\psi(H)})^2]^{-1}(\mathbf{u}_+^{-1}\mathbf{u}_-)^{-1}e^{-\Lambda^+\psi(z)} \\ &\quad [\mathbf{I} - ((\mathbf{u}_+^{-1}\mathbf{u}_-)^{-1}e^{-\Lambda^+[\psi(H)-\psi(z)]})^2]\mathbf{v}_+. \end{aligned} \tag{41}$$

One thing to notice is that the above expressions have redundant matrix groups. For example  $\mathbf{u}_+^{-1}\mathbf{u}_-$  appears several times, but needs to be calculated only once. Moreover,  $\mathbf{v}_+$  and  $\mathbf{v}_-$  can be expressed in terms of  $\mathbf{u}_+$  and  $\mathbf{u}_-$ , through relations (A.10), derived in Appendix A, that we repeat here for convenience:

$$\begin{aligned} \mathbf{v}_+ &= [\mathbf{I} - (\mathbf{u}_+^{-1}\mathbf{u}_-)^2]^{-1}\mathbf{u}_+^{-1}, \\ \mathbf{v}_- &= (\mathbf{u}_+^{-1}\mathbf{u}_-)\mathbf{v}_+. \end{aligned}$$

These relations completely determine the Green’s function matrix. In Section 3.2, we will apply it to compute the contribution to the upwelling radiance at the upper boundary of a scattering and absorbing medium by the lower layers.

### 3. Numerical results

We present two applications of the results obtained in the previous sections. The first uses global reflection and transmission matrices to compute the radiance exiting the upper boundary of a medium via the interaction principle. This approach is computationally more efficient than doubling, particularly for optically thick media, yet achieves a similar degree of accuracy. A

comparison of radiances computed with a doubling code, and the global  $\mathcal{R}$  and  $\mathcal{T}$  derived in the present work is summarized in Section 3.1.

The second numerical application pertains to the computation of the contribution function and the integrated contribution Function, using the Green's function solution, for different profiles of cloud properties. This application is relevant for remote sensing problems where it is important to know the vertical path weighting of the information contained in the radiance measured at the top boundary. The Green's function that we introduced in Section 2.3 is the generalization of the weighting function commonly used in retrievals based on atmospheric thermal emission. In the case when scattering can be neglected and where internal thermal sources are present, the RTE reduces to its scalar form. The weighting function can then be simply recovered by assuming a given form for the extinction coefficient. This results in an analytical, exponential transmission function. When scattering is dominant, as in the case of reflected solar radiation, defining a weighting function is more complicated. The Green's function formulation for the solution of RTE is useful towards defining this weighting function as will be shown in Section 3.2.

### 3.1. Radiance calculations and comparison with the doubling method

Consider a single layer of total optical depth  $\psi(H)$ . Assume the source function is only given by the solar contribution and consider a direct solar beam incident from a direction  $(\mu_\odot, \phi_\odot)$  impinging at the top of the layer. Using Eq. (10) we can evaluate the integral given in (33) and obtain an analytical expression for  $J^\pm$ :

$$J^\pm = \int_0^H \frac{d\psi(z)}{dz} e^{\mathbf{A}[\psi(H)-\psi(z)]} \begin{pmatrix} \Sigma^+ \\ \Sigma^- \end{pmatrix} dz = -e^{\mathbf{A}\psi(H)} S_1^\pm + S_2^\pm, \quad (42)$$

where

$$S_1^\pm = \left( \frac{\mathbf{I}}{\mu_\odot} - \mathbf{A} \right)^{-1} \frac{\omega_0}{4\pi} F_\odot \mathbf{M} \mathbf{P}_\odot^\mp e^{-\psi(H)/\mu_\odot}$$

and

$$S_2^\pm = \left( \frac{\mathbf{I}}{\mu_\odot} - \mathbf{A} \right)^{-1} \frac{\omega_0}{4\pi} F_\odot \mathbf{M} \mathbf{P}_\odot^\mp.$$

According to Eq. (32), the solution for the radiance is given by

$$\begin{pmatrix} I^+(H) \\ I^-(H) \end{pmatrix} = e^{\mathbf{A}\psi(H)} \begin{pmatrix} I^+(0) \\ I^-(0) \end{pmatrix} - e^{\mathbf{A}\psi(H)} \begin{pmatrix} S_1^+ \\ S_1^- \end{pmatrix} + \begin{pmatrix} S_2^+ \\ S_2^- \end{pmatrix}. \quad (43)$$

Rearranging the above expression using the interaction principle as in Eq. (34) we have

$$\begin{aligned} I^+(H) &= \mathcal{T}(0, H) I^+(0) + \mathcal{R}(H, 0) I^-(H) - \mathcal{T}(0, H) S_1^+ \\ &\quad - \mathcal{R}(H, 0) S_2^- + S_2^+, \end{aligned} \quad (44)$$

$$\begin{aligned} I^-(0) &= \mathcal{R}(0, H) I^+(0) + \mathcal{T}(H, 0) I^-(H) \\ &\quad - \mathcal{R}(0, H) S_1^+ + S_1^- - \mathcal{T}(H, 0) S_2^-. \end{aligned} \quad (45)$$

The boundary conditions are

$$I^+(0) = \mathbf{R}_g I^-(0) + \frac{F_\odot}{\pi} A_g e^{-\psi(H)/\mu_\odot}, \quad (46)$$

$$I^-(H) = 0, \quad (47)$$

where we assume that there is no diffuse incoming radiation at the top of the layer and the surface reflection is specified by the matrix  $\mathbf{R}_g$ . For a Lambertian surface,  $\mathbf{R}_g$  has a very simple form with all equal rows, i.e.

$$\mathbf{R}_g = \frac{A_g}{\pi} \begin{pmatrix} w_1 \mu_1 & w_2 \mu_2 & \dots & w_N \mu_N \\ \vdots & \vdots & \vdots & \vdots \end{pmatrix},$$

where  $A_g$  is the ground albedo. For the case of a generic surface, the matrix  $\mathbf{R}_g$  will have a more complicated structure, which has to be specified according to the reflecting properties of the surface. For the case of a completely opaque surface,  $A_g = 0$ . In what follows, we will use this assumption. We are aware of the fact that for optically thin clouds, surface albedo is a major problem in remote sensing using optical channels, and setting  $A_g = 0$  is a simplifying assumption that cannot be made in practice. Nonetheless such assumption is applicable in the presence of thicker clouds or over opaque surfaces such as oceans, and results are still relevant for these cases.

The solution for the radiance field is

$$I^+(H) = \mathcal{T}(0, H) \mathbf{R}_g I^-(0) + \mathcal{T}(0, H) A_g \frac{F_\odot}{\pi} e^{-\psi(H)/\mu_\odot} - \mathcal{T}(0, H) S_1^+ - \mathcal{R}(H, 0) S_2^- + S_2^+, \quad (48)$$

$$I^-(0) = (\mathbf{I} - \mathcal{R}(0, H) \mathbf{R}_g)^{-1} (\mathcal{R}(0, H) A_g \frac{F_\odot}{\pi} e^{-\psi(H)/\mu_\odot} - \mathcal{R}(H, 0) S_1^+ + S_1^+ - \mathcal{T}(H, 0) S_2^-). \quad (49)$$

Note that for each azimuthal component,  $m$ , of the radiance vector (see Eq. (2)) the global reflection and transmission matrices have to be re-evaluated, since they are also azimuthally dependent. There is nothing new here since all the development in the previous sections can be applied for all terms of the azimuthal expansion, provided that eigenvalues and eigenvectors of the  $\mathbf{A}$  matrix are evaluated for all  $m$ .

The phase function used in this study is the Henyey–Greenstein, characterized by the asymmetry parameter  $g$  (see [13]). Standard linear algebra routines (LAPACK, Linear Algebra PACKage [14]) were utilized to compute the eigenvalues and eigenvectors of the  $\mathbf{A}$  matrix. The radiances were computed for  $N = 16$  streams, using Gaussian quadratures. The doubling–adding radiative transfer code used for the comparison of results is documented in Miller et al. [15].

Radiances obtained with the global reflection and transmission have been compared against those from a doubling code, and agreement between these methods was as expected from numerical uncertainties (see Tables 1(a) and (b)). There is, however, one exception to the very

Table 1

Comparison of radiances computed with a doubling code (D) and with the global  $\mathcal{R}$  and  $\mathcal{T}$  technique presented in this study (RT).  $m$  is the index for the expansion terms of the azimuthal series.  $\mu$  represents the cosine of the quadrature angles (observing directions).  $I^+(H)$  and  $I^-(0)$  represent, respectively, the upwelling and downwelling radiances summed up to the  $m$ th term of the azimuth expansion series

$\mu$	$m$	D $I^+(H)$	RT $I^+(H)$	% diff.	D $I^-(0)$	RT $I^-(0)$	% diff.
(a) <i>Optical parameters: <math>\tau = 1</math>, <math>\omega_0 = 1</math>, <math>g = 0</math>, <math>\mu_{\odot} = 0.86</math></i>							
0.9894	0	8.1189E-02	8.1189E-02	0.0	7.3267E-02	7.3315E-02	0.06
0.7554	0	9.4889E-02	9.489E-02	0.0	8.3060E-02	8.3114E-02	0.06
0.0950	0	1.4232E-01	1.4232E-01	0.0	8.3294E-02	8.3382E-02	0.1
(b) <i>Optical parameters: <math>\tau = 1</math>, <math>\omega_0 = 1</math>, <math>g = 0.8</math>, <math>\mu_{\odot} = 0.86</math></i>							
0.9894	0	9.9717E-03	9.9460E-03	0.25	1.6764E-01	1.6752E-01	0.07
0.7554	0	1.6232E-02	1.6209E-02	0.15	1.8942E-01	1.8919E-01	0.12
0.0950	0	4.8565E-02	4.8541E-02	0.25	6.9504E-02	6.8196E-02	1.88
0.9894	3	1.0576E-02	1.0562E-02	0.13	2.8254E-01	2.8223E-01	0.11
0.7554	3	2.1393E-02	2.1344E-02	0.2	6.9865E-01	6.9835E-01	0.04
0.0950	3	8.3972E-02	8.3859E-02	1.34	1.3309E-01	1.3082E-01	1.7
0.9894	7	1.0577E-02	1.0597E-02	0.19	2.8442E-01	2.8408E-01	0.12
0.7554	7	2.1415E-02	2.1382E-02	0.15	8.3781E-01	8.3742E-01	0.05
0.0950	7	8.4466E-02	8.4264E-02	0.24	1.3444E-01	1.3211E-01	1.72
0.9894	11	1.0577E-02	1.0597E-02	0.19	2.8441E-01	2.8408E-01	0.12
0.7554	11	2.1408E-02	2.1402E-02	0.02	8.5923E-01	8.584E-01	0.07
0.0950	11	8.4532E-02	8.4381E-02	0.18	1.3445E-01	1.3218E-01	1.68
0.9894	15	1.0577E-02	1.0597E-02	0.19	2.8441E-01	2.8408E-01	0.12
0.7554	15	2.1406E-02	2.1225E-02	0.84	8.6311E-01	7.7356E-01	10.3
0.0950	15	8.4497E-02	8.4449E-02	0.06	1.3447E-01	1.2792E-01	4.86

close agreement obtained. This applies to a particular set of parameters, corresponding to the case of low quadrature angles ( $\mu < 0.09$ ) in conjunction with conservative scattering ( $\omega_0 \approx 1$ ), an optically thin layer ( $\tau < 1$ ), and a highly forward peaked phase function ( $g \approx 0.85$ ). All other combinations of optical parameters are not affected by this same problem; convergence of the azimuthal cosine series is obtained in most cases with a few expansion terms.

For optically thick media, the calculation of the global reflection and transmission matrices is more efficient than in the doubling method since the number of matrix multiplications is independent of the optical depth of the layer. The total number of matrix multiplications, excluding the computation of the eigenvalues, eigenvectors, and  $\mathcal{R}$  and  $\mathcal{T}$  is 11, regardless of the optical depth of the layer. By comparison, for the doubling method to reach an optical depth of 16 starting from an optical depth  $\Delta\tau = 0.001$ , 28 matrix multiplication are required (14 for  $\mathcal{R}$  and 14 for  $\mathcal{T}$ ), where this figure is derived from the relation  $2^p \Delta\tau = \tau$ , and in our example  $p = 14$ . For this case the eigenmatrix approach will be faster than doubling by more than a factor of two.

We would like to also point out that the present method combines the advantages of the DA, via the introduction of the global reflection and transmission matrices, with the advantages of the eigenmatrix approach. In the case where the boundary conditions change, the new radiances exiting the boundaries of the medium can be computed in a straightforward manner using  $\mathcal{T}$  and  $\mathcal{R}$ , without solving a new BVP as it is required if DISORT is used to perform the calculation. On the other hand, if the optical properties of the layer change, the global reflection and transmission matrices can be recomputed in only 11 matrix multiplications, which will be faster than performing a doubling calculation (once again, this depends on the optical depth of the layer as pointed out in the previous paragraph).

The numerical results above pertain to a single layer atmosphere. Further investigation is necessary to evaluate quantitatively the advantages of the present method of solution over others in the case of a multi-layered medium.

### 3.2. Green’s function results: contribution function and integrated contribution function

In general, the Green’s function solves the integral form of an ordinary differential equation, so we can use it to calculate the solution for the radiance exiting the boundaries of the layer. This application is, however, redundant, since more efficient methods to compute the solution to the RTE have been developed. In this section, we apply the Green’s function form of the solution in a new manner to establish a way of obtaining information about the vertical distribution of the radiance field.

To this end we return to Eq. (34) and express it in terms of the Green’s function matrix derived in that section:

$$\begin{pmatrix} I^+(H) \\ I^-(0) \end{pmatrix} = \begin{pmatrix} \mathcal{T}(0,H) & \mathcal{R}(H,0) \\ \mathcal{R}(0,H) & \mathcal{T}(H,0) \end{pmatrix} \begin{pmatrix} I^+(0) \\ I^-(H) \end{pmatrix} + \int_0^H \begin{pmatrix} \mathbf{G}_{++}(H-z) & \mathbf{G}_{+-}(H-z) \\ \mathbf{G}_{-+}(H-z) & \mathbf{G}_{--}(H-z) \end{pmatrix} \begin{pmatrix} \Sigma^+ \\ \Sigma^- \end{pmatrix} \frac{d\psi(z)}{dz} dz. \tag{50}$$

For simplicity, as was done for the radiance calculations presented in the previous subsection, we assume a non-reflecting lower boundary ( $A_g = 0$ ), so that the homogeneous part of the solution vanishes and Eq. (50) reduces to

$$\begin{pmatrix} I^+(H) \\ I^-(0) \end{pmatrix} = \int_0^H \begin{pmatrix} \mathbf{G}_{++}(H-z) & \mathbf{G}_{+-}(H-z) \\ \mathbf{G}_{-+}(H-z) & \mathbf{G}_{--}(H-z) \end{pmatrix} \begin{pmatrix} \Sigma^+ \\ \Sigma^- \end{pmatrix} \frac{d\psi(z)}{dz} dz. \tag{51}$$

In satellite applications, we are mostly interested in the radiance exiting the upper boundary, so we write it explicitly:

$$I^+(H) = \int_0^H [\mathbf{G}_{++}(H-z)\Sigma^+ + \mathbf{G}_{+-}(H-z)\Sigma^-] \frac{d\psi(z)}{dz} dz. \tag{52}$$

It is clear from (52) that the submatrix  $\mathbf{G}_{++}(H-z)$  is responsible for the redistribution of the upwelling components of the solar source vector ( $\Sigma^+$ ) and  $\mathbf{G}_{+-}(H-z)$  is responsible for the redistribution of the downwelling components of the solar source vector ( $\Sigma^-$ ) into

upwelling radiance. For any particular direction, it is only necessary to examine a single row of the submatrices  $\mathbf{G}_{++}(H - z)$  and  $\mathbf{G}_{+-}(H - z)$  and sum over all  $m$  azimuth components. If, however, the satellite were nadir pointing, then only the  $m = 0$  component would be sufficient to compute the remotely sensed radiances.

The radiance at the top of the atmosphere is the result of the convolution between the Green’s function and the solar source function, so that it is necessary to study this convolution in order to establish what level within the medium mostly influences the observed radiance. We explore this matter with the aid of the *contribution function* and its integral.

We rewrite Eq. (52) as

$$I^+(H) = \int_0^H W(H, z) dz, \tag{53}$$

where

$$W(H, z) = [\mathbf{G}_{++}(H - z)\Sigma^+ + \mathbf{G}_{+-}(H - z)\Sigma^-] \frac{d\psi(z)}{dz} \tag{54}$$

represents the contribution function.

Similarly, we introduce an integrated contribution function as

$$I_W(H, z) = \int_z^H W(H, z') dz'. \tag{55}$$

The integral does not span over the whole layer so that  $I_W$  maintains a  $z$ -dependence. When integrated over the whole depth of the layer (i.e.  $z=0$ ), the radiance exiting the upper boundary is recovered. For any other value  $z$ ,  $I_W$  gives the integrated *contribution* to the upwelling radiance at the top of the layer from all levels below  $H$ . The radiance computed from the Green’s function formulation for the case of a non-reflecting lower boundary (no homogenous solution, but only a particular solution of the RTE) has been compared with previous results from doubling and global  $\mathcal{R}$  and  $\mathcal{T}$  radiance comparison (see Section 3.1). Good agreement has been found, which indicates that our computation of  $W(H, z)$  and its integral is correct.

### 3.3. Examples of reflection from vertically varying clouds

To illustrate an application of the contribution function and the integrated contribution function introduced in the previous section, we examine three hypothetical clouds with the following extinction coefficient profiles:

- (a)  $\sigma_e$  constant with height (homogeneous cloud)
- (b)  $\sigma_e$  increasing linearly with height (“stratus-like” cloud)
- (c)  $\sigma_e$  decreasing linearly with height (“cirrus-like” cloud).

A plot of these extinction profiles is shown in Fig. 1. This cloud classification is arbitrary and is suggested by the fact that stratiform clouds tend to have larger droplets near their top and smaller droplets at their base, hence an extinction coefficient increasing with height, while the converse is true for cirrus clouds. It is clear that there are factors other than the  $\sigma_e$  profile that distinguish stratus from cirrus clouds, in particular the scattering phase function, which renders

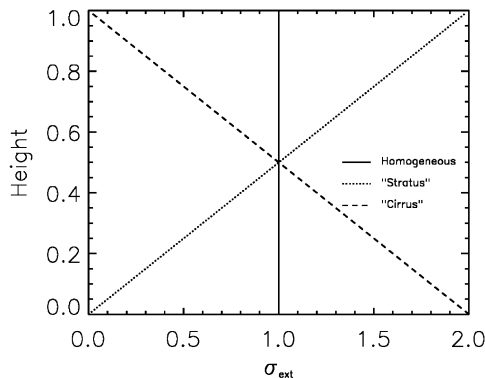


Fig. 1. Vertical profiles of extinction coefficient for three hypothetical clouds (see text for details).

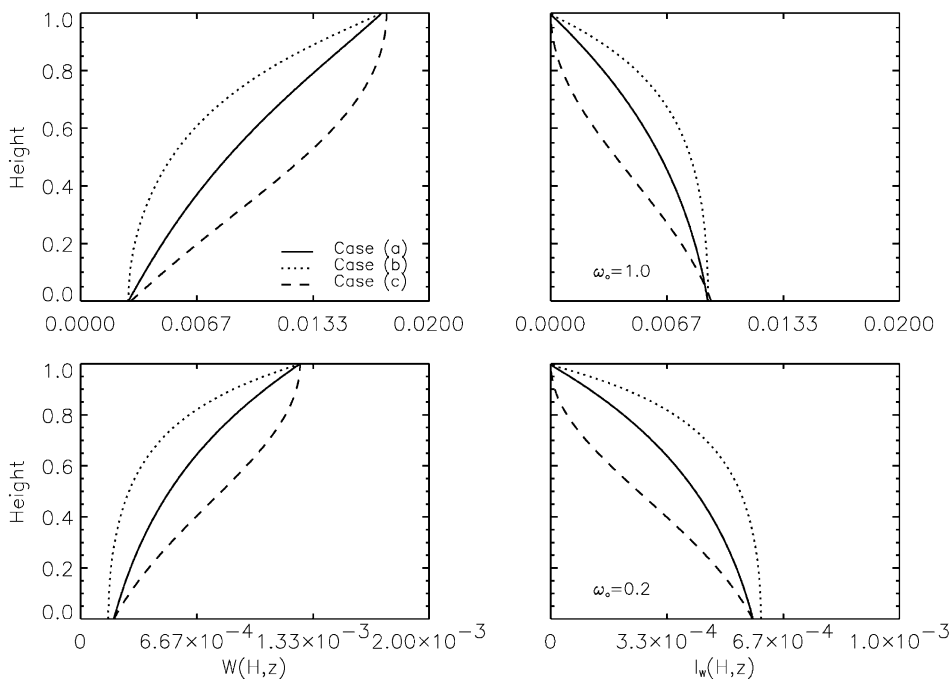


Fig. 2. Profiles of contribution function and integrated contribution function in the direction  $\theta_1 = 8.35^\circ$  for the three cloud scenarios and two different single scattering albedoes, as labeled (upper panels,  $\omega_0 = 1$ ; lower panels,  $\omega_0 = 0.2$ ). See text for explanations. Optical parameters:  $\tau = 1$ ,  $g = 0.8$ . Cosine of solar zenith angle,  $\mu_\odot = 1.0$ .

this representation of the optical properties of these clouds unrealistic. We are also aware that the linear form of the  $\sigma_e$  vertical dependence and the assumption of constant single scattering albedo are limiting factors in our analysis. Nevertheless, we believe that useful insight can be gained by examining the different contribution function and integrated contribution function profiles obtained for each of the three cases.

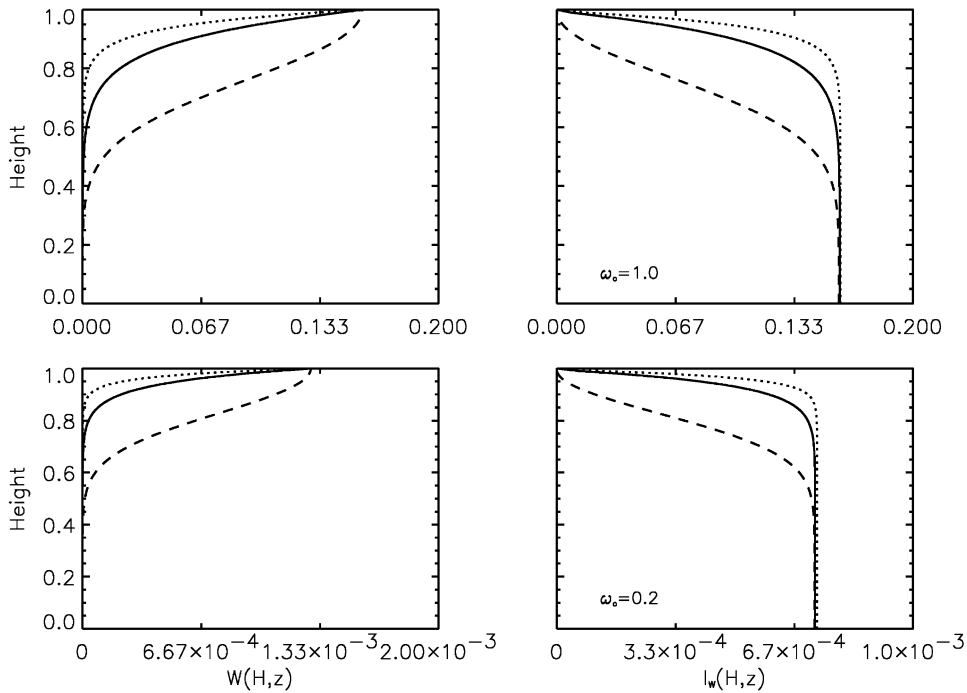


Fig. 3. As in Fig. 2, except  $\tau = 10$ .

We consider two different values of total optical depth,  $\tau = 1$  and  $10$ , and single scattering albedo,  $\omega_0 = 1$  (conservative case) and  $\omega_0 = 0.2$  (nonconservative case). Again an Henyey–Greenstein phase function is used for the calculations, and the asymmetry parameter is fixed at a value of  $0.8$ . We computed profiles of  $W(H,z)$  and  $I_W(H-z)$  for a solar zenith angle of  $0^\circ$  and  $60^\circ$ .

Fig. 2 shows the profiles of  $W(H,z)$  and  $I_W(H-z)$ , for the direction  $\theta_1 = 8.35^\circ$ , for optical depth  $\tau = 1$ . The upper panel is relative to  $\omega_0 = 1.0$  and the lower panel to  $\omega_0 = 0.2$ . The cosine of the solar zenith angle is  $\mu_\odot = 1.0$ . Fig. 3 is the same as Fig. 2, except for an optical depth of  $10$ . If we analyze cases (a) and (b) profiles, we note that the main difference between the two cases resides mainly in the fact that for the  $\tau = 1$  case the contribution function and its integral have non-negligible values throughout the layer, while the  $\tau = 10$  profiles are more concentrated at cloud top, indicating that most of the contribution to the upwelling radiance is coming from the upper portion of the cloud.

A qualitative explanation for this type of behavior lies in the fact that when the medium is optically thin ( $\tau < 1$ ), contributions to the upwelling radiance at the top of the atmosphere involve the entire medium regardless of  $\sigma_e(z)$ . When the optical depth is large, the radiance tends toward saturation. In this case, an additional layer of small optical depth to the base of the medium would negligibly change the radiance at the upper boundary. The situation is different for the “cirrus” cloud (case (c)): the profiles are quite spread out in both cases indicating that contributions to the total radiance are obtained from a larger portion of the cloud, even in the optically thick case, with respect to the stratus and homogeneous cases.

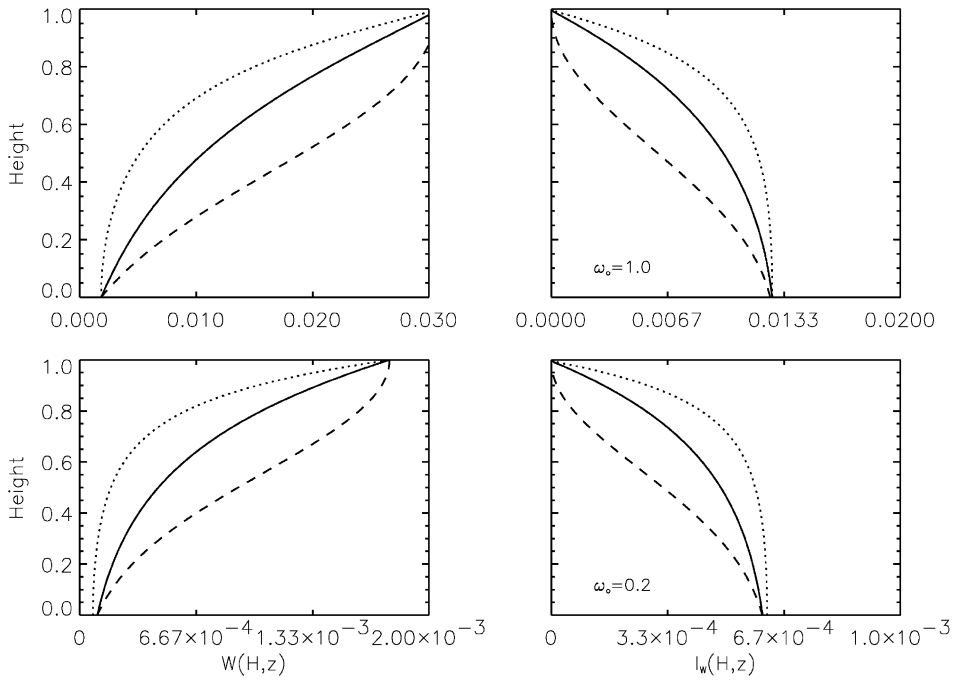


Fig. 4. As in Fig. 2, except  $\mu_{\odot} = 0.5$ .

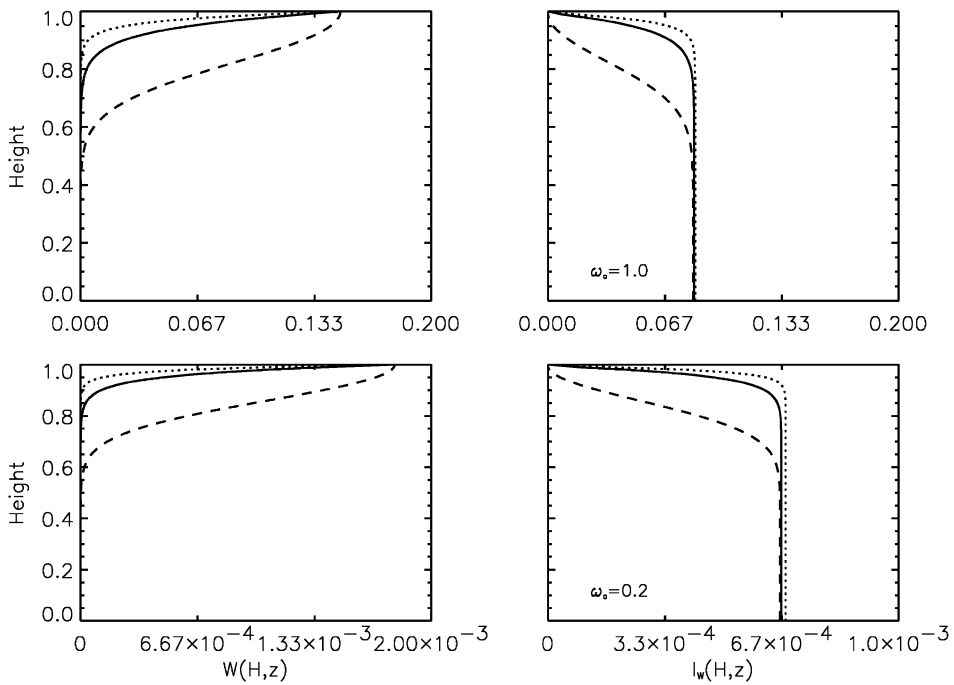


Fig. 5. As in Fig. 2, except  $\tau = 10$  and  $\mu_{\odot} = 0.5$ .

From these results, we conclude that the contribution function and its integral, like the Green's function, are very sensitive to  $\sigma_c(z)$ . This has a strong bearing on retrieval of cloud optical depth when remotely sensing different cloud types. It appears that the information that one retrieves from radiance measurements at the top of the layer comes preferentially from different levels, according to the type of cloud that it is being sensed.

An analogous trend is also evident in the non-conservative case as shown in the lower panels of Figs. 2 and 3. The major difference with respect to the conservative case lies in the magnitude of the contributions (note that the horizontal scales change from panel to panel). Although the shape of the profile is similar to the conservative case, in the non-conservative case the amplitude of the two functions is noticeably smaller.

Similar conclusions can be drawn for the case of a solar zenith angle of  $60^\circ$  ( $\mu_\odot = 0.5$ ) (Figs. 4 and 5) as far as the vertical distribution of the contribution goes for the three cloud scenarios. The major difference resides in the magnitude of the contributions in the conservative cases. In the  $\tau=1$  conservative case (Fig. 4, upper panel), the magnitude of the contributions is larger with respect to the corresponding case for  $\mu_\odot = 1$  (Fig. 2, upper panel). In contrast, for the  $\tau=10$  conservative case (Fig. 5, upper panel), the magnitude is smaller with respect to the corresponding case for  $\mu_\odot = 1$  (Fig. 3, upper panel). For the non-conservative case, comparing the lower panels of Figs. 2 and 4 and Figs. 3 and 5, no major differences can be noted between the  $\mu_\odot = 1$  and 0.5 examples. This is due to the fact that for absorbing media, the increase in optical path traveled by the photons due to absorption is more dramatic than the increase in optical path due to a lower solar zenith angle.

#### 4. Further applications: the penetration optical depth

With the function  $I_W(H-z)$  introduced in Section 3.2 we can quantify the percentage of the total upwelling radiance associated with a layer extending downward from the top of the cloud to some reference level  $z'$ . Define the optical depth of the layer  $(z', H)$  by  $\tau_p$ . This *penetration* optical depth,  $\tau_p$ , is a useful way of understanding what portions of the cloud contribute to the measured radiance at cloud top as described by Platnick (2).

Fig. 6 shows a contour plot of  $\tau_p$  versus the total cloud optical depth  $\tau$  of the layer (horizontal axis) and the percentage of total radiance at the upper boundary (vertical axis), for a single scattering albedo of 1 (upper panel) and 0.2 (lower panel) for the homogeneous cloud. The solar zenith angle is  $0^\circ$ . Note that when the percentage is 100%,  $\tau_p$  equals  $\tau$ . The conservative and non-conservative cases yield different results in terms of  $\tau_p$ . For example, if the total optical depth is 4, 90% of the total radiance emerges from the layer of optical depth approximately equal to 1.6 when  $\omega_0=1$ . For the same percentage and total optical depth,  $\tau_p \approx 1.1$  for  $\omega_0=0.2$ . This indicates that absorption reduces the level of penetration within the cloud, leading to a more concentrated contribution near cloud top. This result is also shown in the previous section with the profiles of  $W(H,z)$  and  $I_W(H,z)$ . At higher solar zenith angle,  $60^\circ$ , a similar trend is observed (see Fig. 7). The increase of solar zenith angle contributes to the reduction of the penetration optical depth because the path length the photons travel is increased by  $1/\mu_\odot$ , where  $\mu_\odot$  is the cosine of the solar zenith angle. This increases the probability of absorption or scattering. For the same example considered before, i.e. total  $\tau = 4$  and percentage of total

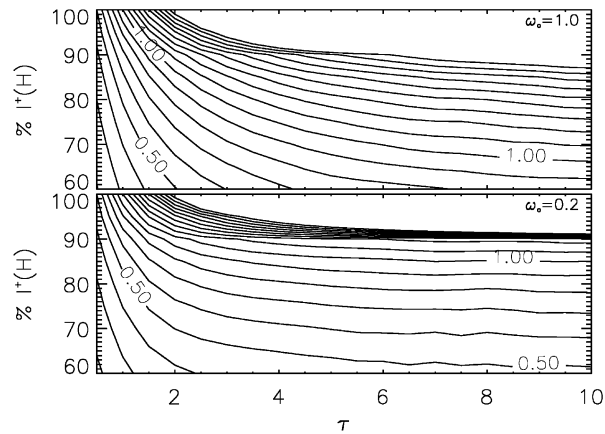


Fig. 6. Contour plot of penetration optical depth ( $\tau_p$ ) as a function of total optical depth and percentage of upwelling radiance at the upper boundary. Two single scattering albedos are shown:  $\omega_0 = 1$  (upper panel) and  $\omega_0 = 0.2$  (lower panel). The cosine of the solar zenith angle is 1.0.

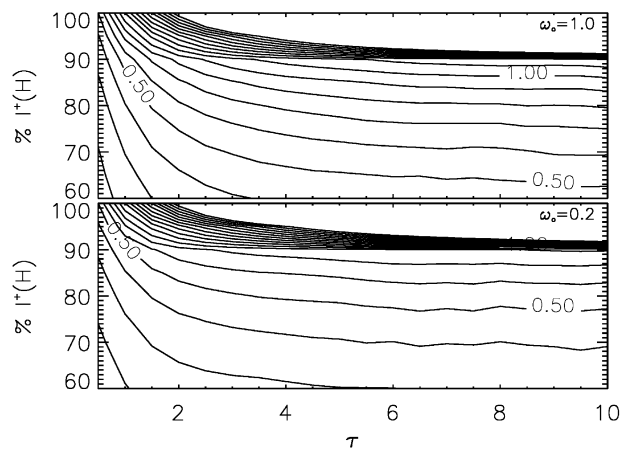


Fig. 7. As in Fig. 6, except the cosine of solar zenith angle is 0.5.

radiance equal to 90%,  $\tau_p \approx 1.1$  in the conservative case and  $\tau_p \approx 0.7$  in the non-conservative case.

The penetration optical depth is the same for the three clouds considered, indicating that it is not possible to discriminate between clouds of different types only from a measurement of the reflected radiance at the top of the atmosphere, unless an assumption is made concerning the form of the extinction coefficient, or multispectral measurements are also performed. For example multi-spectral measurements can be taken over a very narrow spectral interval where the cloud particles scatter conservatively (e.g.  $\omega_0 = 1$ ), but where the surrounding atmospheric gas exhibits strong variations in absorption as in the case of the oxygen A-band (750–760 nm).

This requires additional information about the cloud height and thickness such as may be provided by an active instrument (e.g. radar). Alternatively, measurements can be performed in various region of the spectrum at different wavelengths where there is negligible absorption by atmospheric gases but strong variations of  $\omega_0$  of the cloud particles.

## 5. Summary and conclusions

Properties of sunlight scattered from vertically inhomogeneous media have been investigated using a Green's function approach. The eigenmatrix solution of the RTE in concert with the interaction principle have been explored in a new way to obtain the Green's function matrix. To achieve a general and stable form of the Green's function, stabilization of global reflection and transmission matrices, derived from the eigenmatrix, was performed. Radiances computed with the resultant stable global  $\mathcal{R}$  and  $\mathcal{T}$ , for a range of optical depths, single scattering albedoes and asymmetry parameters, are in excellent agreement with those calculated from a doubling code.

By definition, the Green's function, when weighted by the source function in the form of a convolution, produces the solution of the RTE. From this form of solution, with the aid of the Green's function we introduced the contribution function and its integral to show the distribution of the vertical weighting for different extinction profiles. To explore this aspect, we used a homogenous cloud ( $\sigma_e$  constant with height), a "stratus-like" cloud ( $\sigma_e$  increasing linearly with height) and a "cirrus-like" cloud ( $\sigma_e$  decreasing linearly with height), in all cases maintaining constant  $\omega_0$  and constant total  $\tau$ . Analysis of profiles of the contribution function and the integrated contribution function has shown that the vertical weighting is sensitive to the extinction profile as well as to the single scattering albedo and to the solar zenith angle.

With the aid of the integrated contribution function, the concept of *penetration* optical depth, that is, the optical depth at which a given percentage of the radiance measured at cloud top is recovered, was introduced. It was found that the penetration optical depth is a strong function of single scattering albedo and solar zenith angle, but is insensitive to the extinction profile. This contrasts with the *effective level* of contribution, which is sensitive to the extinction profile. In particular, for a given penetration optical depth, the corresponding penetration depth is generally greater for cirrus clouds than for the other two clouds considered, since the extinction increases from cloud top down at a lower rate than for the stratus and the homogeneous cloud.

These results suggest that information recovered from path integrated measurements, such as visible upwelling radiances at the top of the atmosphere observed by a satellite instrument, originates from specific regions within the cloud and is dependent on the type of cloud sensed. This study provides a quantitative method for assessing the level from which the information is mainly coming, provided some educated guess can be made about the cloud scene being observed and the type of extinction profile such a cloud might have. The method introduced in this paper, when combined with profile information provided by active sensors, may lead to a more definitive way of retrieving extinction profiles in cloud.

### Acknowledgements

This research has been supported under Department of Energy Research Grant DE-FG03-94ER61748 and CloudSat NASA Contract #NAS5-99237. We wish to thank Dr. Steve Miller for providing the radiance results for the comparison from his doubling code, Mick Hopsecger for double-checking the algebra, and Tristan L’Ecuyer for suggesting a compact matrix form to incorporate the surface reflection.

### Appendix A.

Consider the eigenvalue problem in the vector form

$$\mathbf{A}\vec{x}_r = \lambda_r \vec{x}_r, \tag{A.1}$$

where  $\lambda_r$  is a generic eigenvalue of  $\mathbf{A}$  and  $\vec{x}_r$  is the eigenvector associated.

If we choose to write  $\vec{x}_r$  as constituted of two vectors of dimension  $N$ ,  $\vec{u}_r$  and  $\vec{v}_r$  we have

$$\begin{pmatrix} \mathbf{t} & -\mathbf{r} \\ \mathbf{r} & -\mathbf{t} \end{pmatrix} \begin{pmatrix} \vec{u}_r \\ \vec{v}_r \end{pmatrix} = \lambda_r \begin{pmatrix} \vec{u}_r \\ \vec{v}_r \end{pmatrix}, \tag{A.2}$$

which can be written as

$$\begin{aligned} \mathbf{t}\vec{u}_r - \mathbf{r}\vec{v}_r &= \lambda_r \vec{u}_r, \\ \mathbf{r}\vec{u}_r - \mathbf{t}\vec{v}_r &= \lambda_r \vec{v}_r. \end{aligned} \tag{A.3}$$

Summing and subtracting the above equations, we get

$$\begin{aligned} (\mathbf{t} + \mathbf{r})(\vec{u}_r - \vec{v}_r) &= \lambda_r(\vec{u}_r + \vec{v}_r), \\ (\mathbf{t} - \mathbf{r})(\vec{u}_r + \vec{v}_r) &= \lambda_r(\vec{u}_r - \vec{v}_r). \end{aligned} \tag{A.4}$$

Multiply the first row of (A.4) by  $(\mathbf{t} - \mathbf{r})$  and the second row by  $(\mathbf{t} + \mathbf{r})$ . Upon rearrangement,

$$\begin{aligned} (\mathbf{t} - \mathbf{r})(\mathbf{t} + \mathbf{r})(\vec{u}_r - \vec{v}_r) &= \lambda_r^2(\vec{u}_r - \vec{v}_r), \\ (\mathbf{t} + \mathbf{r})(\mathbf{t} - \mathbf{r})(\vec{u}_r + \vec{v}_r) &= \lambda_r^2(\vec{u}_r + \vec{v}_r). \end{aligned} \tag{A.5}$$

If we introduce the new matrices and vectors

$$\begin{aligned} \mathbf{B} &= (\mathbf{t} - \mathbf{r})(\mathbf{t} + \mathbf{r}), \quad \mathbf{C} = (\mathbf{t} + \mathbf{r})(\mathbf{t} - \mathbf{r}), \\ \vec{d}_r &= \vec{u}_r - \vec{v}_r, \quad \vec{s}_r = \vec{u}_r + \vec{v}_r, \end{aligned}$$

we obtain two new eigenvalue problems:

$$\begin{aligned} \mathbf{B}\vec{d}_r &= \lambda_r^2 \vec{d}_r, \\ \mathbf{C}\vec{s}_r &= \lambda_r^2 \vec{s}_r. \end{aligned} \tag{A.6}$$

The eigenvalues of the matrix **A** are simply the square root of the eigenvalues of either the matrix **B** or **C**. Having computed the eigenvalues and eigenvectors of, say, the matrix **B** we can recover the eigenvalues and eigenvectors of **A**. From the first equation of the system in (A.4), the vector  $\vec{s}_r$ , eigenvector of **C** can be expressed in terms of the vector  $\vec{d}_r$ ,

$$\vec{s}_r = \frac{(\mathbf{t} + \mathbf{r})}{\lambda_r} \vec{d}_r,$$

from which follows:

$$\begin{aligned} \vec{u}_r - \vec{v}_r &= \vec{d}_r, \\ \vec{u}_r + \vec{v}_r &= \frac{(\mathbf{t} + \mathbf{r})}{\lambda_r} \vec{d}_r \end{aligned} \tag{A.7}$$

or

$$\begin{aligned} \vec{u}_r &= \frac{1}{2} \left[ \mathbf{I} + \frac{(\mathbf{t} + \mathbf{r})}{\lambda_r} \right] \vec{d}_r, \\ \vec{v}_r &= \frac{1}{2} \left[ -\mathbf{I} + \frac{(\mathbf{t} + \mathbf{r})}{\lambda_r} \right] \vec{d}_r. \end{aligned} \tag{A.8}$$

Since  $\lambda_r$  can be positive or negative, we have another set of equations for  $\lambda_r < 0$ :

$$\begin{aligned} \vec{u}_r &= \frac{1}{2} \left[ \mathbf{I} - \frac{(\mathbf{t} + \mathbf{r})}{|\lambda_r|} \right] \vec{d}_r, \\ \vec{v}_r &= \frac{1}{2} \left[ -\mathbf{I} - \frac{(\mathbf{t} + \mathbf{r})}{|\lambda_r|} \right] \vec{d}_r. \end{aligned} \tag{A.9}$$

Inspection discloses that  $\vec{v}_r$  corresponding to  $\lambda_r > 0$  is equal to  $-\vec{u}_r$  for  $\lambda_r < 0$ . Similarly,  $\vec{v}_r$  corresponding to  $\lambda_r < 0$  is equal to  $-\vec{u}_r$  associated with  $\lambda_r > 0$ . This implies that we only have to compute  $\vec{u}_r$  for both  $\lambda_r$  positive and negative to obtain the full eigenvector matrix.

Let  $\mathbf{u}_+$  be the matrix whose columns are the vectors  $\vec{u}_r$  for  $\lambda_r > 0$  and  $\mathbf{u}_-$  the matrix whose columns are vectors  $\vec{u}_r$  for  $\lambda_r < 0$ .

Thus, the matrix **X** takes the following form:

$$\mathbf{X} = \begin{pmatrix} \mathbf{u}_+ & \mathbf{u}_- \\ -\mathbf{u}_- & -\mathbf{u}_+ \end{pmatrix}.$$

It can be shown that the inverse of **X**,  $\mathbf{X}^{-1}$ , has a similar form:

$$\mathbf{X}^{-1} = \begin{pmatrix} \mathbf{v}_+ & \mathbf{v}_- \\ -\mathbf{v}_- & -\mathbf{v}_+ \end{pmatrix}$$

and the elements of  $\mathbf{X}^{-1}$  can be computed from the elements of **X** using the following matrix relationships:

$$\begin{aligned} \mathbf{v}_+ &= [\mathbf{I} - (\mathbf{u}_+^{-1} \mathbf{u}_-)^2]^{-1} \mathbf{u}_+^{-1}, \\ \mathbf{v}_- &= (\mathbf{u}_+^{-1} \mathbf{u}_-) \mathbf{v}_+ \end{aligned} \tag{A.10}$$

obtained from  $\mathbf{X}\mathbf{X}^{-1} = \mathbf{X}^{-1}\mathbf{X} = \mathbf{I}$ .

**Appendix B.**

Beginning with the form of the matrix exponential derived in Section 2.1.3, we derive a stable semi-analytical expression for the global reflection and transmission operators.

Starting from Eq. (28), we rewrite it explicitly as

$$\begin{aligned} \mathcal{T}(H, 0) &= \mathbf{e}_{22}^{-1}(H) \\ &= (-\mathbf{u}_- e^{\Lambda^+ \psi(H) \mathbf{v}_-} + \mathbf{u}_+ e^{-\Lambda^+ \psi(H) \mathbf{v}_+})^{-1}. \end{aligned} \tag{B.1}$$

Rearranging

$$\begin{aligned} \mathcal{T}(H, 0) &= \{(-\mathbf{u}_- e^{\Lambda^+ \psi(H) \mathbf{v}_-})[\mathbf{I} - (\mathbf{u}_- e^{\Lambda^+ \psi(H) \mathbf{v}_-})^{-1}(\mathbf{u}_+ e^{-\Lambda^+ \psi(H) \mathbf{v}_+})]\}^{-1} \\ &= [\mathbf{I} - (\mathbf{u}_- e^{\Lambda^+ \psi(H) \mathbf{v}_-})^{-1}(\mathbf{u}_+ e^{-\Lambda^+ \psi(H) \mathbf{v}_+})]^{-1}(-\mathbf{u}_- e^{\Lambda^+ \psi(H) \mathbf{v}_-})^{-1} \\ &= -[\mathbf{I} - \mathbf{Q}_1]^{-1} \mathbf{Q}_2^{-1}, \end{aligned} \tag{B.2}$$

where

$$\begin{aligned} \mathbf{Q}_1 &= (\mathbf{u}_- e^{\Lambda^+ \psi(H) \mathbf{v}_-})^{-1}(\mathbf{u}_+ e^{-\Lambda^+ \psi(H) \mathbf{v}_+}), \\ \mathbf{Q}_2 &= (\mathbf{u}_- e^{\Lambda^+ \psi(H) \mathbf{v}_-}). \end{aligned}$$

Expanding the term  $[\mathbf{I} - \mathbf{Q}_1]^{-1}$  in series we have

$$\mathcal{T}(H, 0) = -[\mathbf{I} + \mathbf{Q}_1 + \mathbf{Q}_1^2 + \mathbf{Q}_1^3 + \dots] \mathbf{Q}_2^{-1}. \tag{B.3}$$

By using the expressions for  $\mathbf{v}_\pm$  derived in Section 2.1.3,  $\mathbf{Q}_1$  and  $\mathbf{Q}_2$  can be manipulated to yield

$$\begin{aligned} \mathbf{Q}_1 &= \mathbf{u}_+ [\mathbf{I} - (\mathbf{u}_+^{-1} \mathbf{u}_-)^2] [(\mathbf{u}_+^{-1} \mathbf{u}_-)^{-1} e^{-\Lambda^+ \psi(H)}]^2 \{\mathbf{u}_+ [\mathbf{I} - (\mathbf{u}_+^{-1} \mathbf{u}_-)^2]\}^{-1}, \\ \mathbf{Q}_2^{-1} &= \mathbf{u}_+ [\mathbf{I} - (\mathbf{u}_+^{-1} \mathbf{u}_-)^2] [(\mathbf{u}_+^{-1} \mathbf{u}_-)^{-1} e^{-\Lambda^+ \psi(H)}] \mathbf{u}_-^{-1}. \end{aligned}$$

Substituting in (B.3) and re-summing the geometric series, we obtain the following expression for  $\mathcal{T}$ , which involves only *decaying* exponentials:

$$\mathcal{T}(H, 0) = -\mathbf{u}_+ [\mathbf{I} - (\mathbf{u}_+^{-1} \mathbf{u}_-)^2] [(\mathbf{u}_+^{-1} \mathbf{u}_-)^{-1} e^{-\Lambda^+ \psi(H)}] \{\mathbf{I} - [(\mathbf{u}_+^{-1} \mathbf{u}_-)^{-1} e^{-\Lambda^+ \psi(H)}]^2\}^{-1} \mathbf{u}_-^{-1}. \tag{B.4}$$

In a similar way, we can compute a stable form of the global reflection matrix,  $\mathcal{R}$ , starting from Eq. (27):

$$\begin{aligned} \mathcal{R}(H, 0) &= \mathbf{e}_{12}(H) \mathbf{e}_{22}^{-1}(H) \\ &= (\mathbf{u}_+ e^{\Lambda^+ \psi(H) \mathbf{v}_-} - \mathbf{u}_- e^{-\Lambda^+ \psi(H) \mathbf{v}_+}) (-\mathbf{u}_- e^{\Lambda^+ \psi(H) \mathbf{v}_-} + \mathbf{u}_+ e^{-\Lambda^+ \psi(H) \mathbf{v}_+})^{-1}. \end{aligned} \tag{B.5}$$

The stable form for  $\mathcal{T}$  derived above leads to a stable form for the global reflection matrix  $\mathcal{R}$ .

$$\begin{aligned} \mathcal{R}(H, 0) &= -\mathbf{u}_+ [\mathbf{I} - (\mathbf{u}_+^{-1} \mathbf{u}_-) e^{-\Lambda^+ \psi(H)} (\mathbf{u}_+^{-1} \mathbf{u}_-)^{-1} e^{-\Lambda^+ \psi(H)}] \\ &\quad \{\mathbf{I} - [(\mathbf{u}_+^{-1} \mathbf{u}_-)^{-1} e^{-\Lambda^+ \psi(H)}]^2\}^{-1} \mathbf{u}_-^{-1}. \end{aligned} \tag{B.6}$$

## References

- [1] Nakajima T, King MD. *J Atmos Sci* 1990;47:1878.
- [2] Platnick S. *J Geophys Res* 2000;105 D18:22,919.
- [3] Lenoble J. *Radiative transfer in scattering and absorbing atmospheres: standard computational procedures*. Hampton, VA: Deepak Publishing, 1985.
- [4] van de Hulst AC. *A new look at multiple scattering*, Technical Report. New York: NASA Institute for Space Studies, 1962.
- [5] Irvine WM. *Icarus* 1975;25:175.
- [6] Stamnes K, Tsay S-C, Wiscombe WJ, Jayaweera K. *Appl Opt* 1988;27:2502.
- [7] Chandrasekar S. *Radiative transfer*. New York: Dover, 1960.
- [8] Waterman PC. *J Opt Soc Am* 1981;71:410.
- [9] Kalkofen W. *Numerical radiative transfer*. Cambridge: Cambridge University Press, 1985.
- [10] Mobley CD. *Light and water*. San Diego: Academic Press, 1995.
- [11] Kuscer I, Vidav I. *J Math Anal Appl* 1969;25:80.
- [12] Stamnes K, Conklin P. *JQSRT* 1984;31:273.
- [13] Liou K-N. *An introduction to atmospheric radiation*. New York: Academic Press, 1980.
- [14] Anderson E, Bai Z, Bishof C, Blackford S, Demmel J, Dongarra J, Du Croz J, Greenbaum A, Hammarling S, McKenney A, Sorensen D. *LAPACK Users's guide*, 3rd ed. Philadelphia: SIAM, 1999.
- [15] Miller SD, Stephens GL, Drummond CK, Heidinger AK, Partain PT. *J Geophys Res* 2000;105 D15:19,955.